Direct calculation of Slater-Koster parameters: Fourfold-coordinated silicon/boron phases

A. K. McMahan and J. E. Klepeis
Lawrence Livermore National Laboratory, University of California, Livermore, California 94550
(Received 28 May 1997)

The need for tight-binding total-energy representations of interatomic forces has renewed interest in Slater-Koster parametrization of electron band structure. For larger numbers of parameters, as in multicomponent systems, and to truly test issues of transferability, it is advantageous to have means of directly calculating these parameters. Here we derive analytic expressions for the two-center Slater-Koster hopping parameters, effective site energies, and effective crystal-field parameters in terms of the one-electron Hamiltonian *matrix* elements in any localized minimal basis, and analogous quantities for the overlap. We apply these expressions to the cubic diamond phases of Si and B, and the zinc-blende phase of SiB at three volumes each, using spd, nonorthogonal full potential linear muffin-tin orbital matrix elements calculated with a linked or contracted minimal basis. [S0163-1829(97)08243-X]

I. INTRODUCTION

The use of tight-binding formalism to parametrize electron band structures dates from the early work of Slater and Koster,[1] and has continued to the present.[2–6] When supplemented with information as to how the associated parameters vary with interatomic separation, and usually also by explicit interatomic potentials, one can construct total-energy functionals of the atomic positions.[7–18] There has been considerable interest in such tight-binding total-energy representations to provide interatomic forces for structural relaxation[7] and for molecular-dynamics simulations.[19] In much of this work, parametrized functional forms or splines defining the interatomic separation dependence of the various Slater-Koster parameters and interatomic potentials are fit by nonlinear minimization to an *ab initio* data base of band structures and total energies. Interesting developments include the use of non-pairwise-additive functional forms for the interatomic potentials and Slater-Koster interactions,[11–14] augmentation of the *ab initio* data base by forces,[15] and the use of local-environment-dependent site energies,[16–18] sometimes in place of interatomic potentials.[18]

As the number of required parameters grows roughly quadratically with the number of chemical species in multicomponent systems, and in order to truly test issues of transferability, it is useful to have means of directly calculating Slater-Koster parameters. Andersen and co-workers implemented a basis of screened muffin-tin orbitals to create a two-center formulation of the one-electron problem within the atomic sphere approximation,[20] which has been used to extract Slater-Koster parameters for orthogonal representations.[21] Porezag *et al.* calculated nonorthogonal Slater-Koster parameters using a basis of slightly contracted pseudoatom eigenfunctions,[22] and generated successful tight-binding total-energy representations for a number of multicomponent systems using such parameters.[23]

It is the purpose of the present paper to demonstrate that any *ab initio* band-structure method which is implemented with a localized basis, or can be projected onto such a basis,[24] can also be used to provide a simple and direct calculation of the associated Slater-Koster parameters given the **k**-dependent Hamiltonian *matrix elements*, and similarly for the overlap. We derive analytic expressions which uniquely define the two-center Slater-Koster hopping parameters in terms of these matrix elements. Moreover, by assembling the matrices from a linked or contracted minimal basis, i.e., by using optimized fixed linear combinations of a larger set of basis functions employed by the *ab initio* band-structure code, one may obtain Slater-Koster representations of accuracy approaching that obtained from fits to the one-electron eigenvalues.[6] Our approach is purely deterministic, without the need for any fitting. In this way we are able to avoid the problems associated with multiple local minima, which means that the additional effort to calculate parameters for many component systems is minimal. Furthermore, we can now directly study effects such as making the two-center approximation, and obtain additional insights concerning the general characteristics of the parameters themselves.

Site energies and crystal-field interactions are also essential parts of two-center representations of electron band structure. While the true or bare site energies and crystal-field parameters are underdetermined by the matrix elements for a single structure, the Hamiltonian for a given structure behaves as if it were characterized by generally a small number of *effective* site energies and crystal-field interactions which *can* be determined, along with definitions of these effective parameters in terms of sums over the bare crystal-field interactions. Both the effective site energies, which are the usual site energies which would be obtained by fits to the band structure, and the effective crystal-field interactions vary with local environment due to these structure-dependent expansions.[16,17] Moreover, by a simple transformation of the crystal-field parameters, we demonstrate the formal similarity of the effective site energy expansions to sums over interatomic potentials, which justifies the trade-off between interatomic potentials and environmental-dependent site energies in recent work.[18]

As an application of the present method, we calculated the Slater-Koster parameters at three different volumes for the cubic diamond phases of Si and B, and for zinc-blende SiB. The resultant hopping parameters are relatively transferable over these chemical and atomic-volume variations for

fourfold-coordinated phases. However, preliminary tests for other structures suggest some coordination dependence to the hopping parameters, so that environment-dependent functional forms[14] may be needed for a transferable representation of these *ab initio* parameters. This is beyond the scope of the present paper, for which the primary focus is the method for calculating the tight-binding parameters. In this regard it is to be emphasized that our directly calculated parameters give a comparable, and reasonably accurate, representation of the band structure for all phases and all coordinations considered.

Our choice of the silicon-boron system has been motivated in part by concern over boron diffusion in Si-based semiconductor devices during fabrication, which is an issue of some importance as feature sizes are increasingly reduced. Significant insight into the atomic-scale migration mechanisms has been achieved with *ab initio* local-density-functional methods;[25] however, these methods become too expensive for systematic investigation of larger B aggregates in Si, and so a tight-binding total-energy representation would be valuable. While silicon-boron interactions have been added[26] to a near-neighbor, sp, orthogonal tight-binding total-energy representation for Si,[9] and successfully used to examine single B impurities in Si,[27] additional B-B interactions would be needed for larger B aggregates. Further extension of a Si/B representation to the ternary Si/B/H system would also enable simulation of the deposition processes for p-type material using diborane and silane.

In the remainder of this paper we describe the method of calculating the Slater-Koster parameters in Sec. II, details of the full potential linear muffin-tin orbital (FP-LMTO) method used here in Sec. III, and our numerical results in Sec. IV. We present a summary in Sec. V.

II. CALCULATION OF SLATER-KOSTER PARAMETERS

The Slater-Koster parameters may be calculated directly from minimal basis, one-electron Hamiltonian, **k**-dependent *matrix elements* for a suitable localized basis. In this section we show that even when imposing the common two-center approximation, there are closed-form expressions which relate the Slater-Koster hopping parameters to unique linear combinations of these matrix elements. Crystal-field terms can be obtained in a similar manner. In contrast to the hopping parameters, however, only specific sums of the crystal-field parameters over atomic shells may be determined for a given structure. Our approach is similar in spirit to calculating the Slater-Koster matrix elements directly, as in a linear combination of atomic orbitals approach, but there are a number of advantages which will become evident below.

Matrix elements of the one-electron Hamiltonian may be written

$$H^{\mathbf{k}}_{\mathbf{q}lm,\mathbf{q}'l'm'}=H^{0}_{\mathbf{q}lm,\mathbf{q}l'm'}\delta_{\mathbf{q}\mathbf{q}'}+\Delta H^{\mathbf{k}}_{\mathbf{q}lm,\mathbf{q}'l'm'}, \tag{1}$$

separating intrasite and intersite terms,

$$H^{0}_{\mathbf{q}lm,\mathbf{q}l'm'}=\langle 0\mathbf{q}lm|H|0\mathbf{q}l'm'\rangle, \tag{2}$$

$$\Delta H^{\mathbf{k}}_{\mathbf{q}lm,\mathbf{q}'l'm'}=\sum_{\mathbf{R}}^{\mathbf{R}+\mathbf{q}'\neq\mathbf{q}} e^{i\mathbf{k}\cdot\mathbf{R}}\langle 0\mathbf{q}lm|H|\mathbf{R}\mathbf{q}'l'm'\rangle, \tag{3}$$

respectively, which implies

$$H^{0}_{\mathbf{q}lm,\mathbf{q}l'm'}=\frac{1}{N}\sum_{\mathbf{k}} H^{\mathbf{k}}_{\mathbf{q}lm,\mathbf{q}l'm'}. \tag{4}$$

Here $|\mathbf{R}\mathbf{q}lm\rangle$ represents an orbital of angular and magnetic quantum numbers l and m, respectively, at location $\mathbf{R}+\mathbf{q}$, with $\mathbf{R}$ a Bravais lattice vector, and $\mathbf{q}$ a basis vector. Basis vectors will also have an associated type τ to distinguish equivalent from inequivalent sites, for example the two different sites ($\mathbf{q}_1\neq\mathbf{q}_2$) which are equivalent ($\tau_1=\tau_2$) in cubic diamond but inequivalent ($\tau_1\neq\tau_2$) in the zinc-blende structure.

In the remainder of this section, we describe Slater-Koster expansions for the two terms given by Eqs. (2) and (3), beginning with the latter. The expansion of $\mathbf{H}^0$ is in terms of site energies, ε, and crystal-field parameters, χ; while that for $\Delta\mathbf{H}^{\mathbf{k}}$ is in terms of intersite hopping parameters, t. Analogous expansions exist for the overlap matrix, where we denote the hopping parameters by s. For bases which are *on-site* orthonormal, $\mathbf{O}^0$ is the identity, so that site energy analogs are unity, while crystal-field analogs are zero.

A. Hopping parameters

In the two-center approximation[1,6] one assumes that (i) the potential terms in the one-electron operator H may be represented as a sum of spherical potentials centered about the various atom sites, and (ii) that three-center integrals can be ignored. If this approximation is imposed, Eq. (3) may be expanded in Slater-Koster hopping parameters $t_{\tau\tau' ll'\mu}(d)$, where τ is the type of atom at basis position $\mathbf{q}$, and $\mu=0,\ldots,\min(l,l')$ is the magnetic quantum number about the interatomic axis $\mathbf{R}+\mathbf{q}'-\mathbf{q}$,

$$\Delta H^{\mathbf{k}}_{\mathbf{q}lm,\mathbf{q}'l'm'}\approx\sum_{\mathbf{R}}^{\mathbf{R}+\mathbf{q}'\neq\mathbf{q}} e^{i\mathbf{k}\cdot\mathbf{R}}\sum_{\mu} g_{\mu}(lm,l'm',\widehat{\mathbf{R}+\mathbf{q}'-\mathbf{q}}) \times t_{\tau\tau' ll'\mu}(|\mathbf{R}+\mathbf{q}'-\mathbf{q}|) \tag{5}$$

$$\approx\sum_{n}^{\mathbf{q},\mathbf{q}'}\sum_{\mu} G^{\mathbf{k}}_{n\mu}(lm,l'm')t_{\tau\tau' ll'\mu}(d_n). \tag{6}$$

Here,

$$G^{\mathbf{k}}_{n\mu}(lm,l'm') \equiv\sum_{\mathbf{R}}^{|\mathbf{R}+\mathbf{q}'-\mathbf{q}|=d_n} e^{i\mathbf{k}\cdot\mathbf{R}}g_{\mu}(lm,l'm',\widehat{\mathbf{R}+\mathbf{q}'-\mathbf{q}}), \tag{7}$$

and Eq. (6) reformulates the expansion in terms of shells, n, of atoms $\mathbf{R}+\mathbf{q}'$ at distance $d_n\equiv|\mathbf{R}+\mathbf{q}'-\mathbf{q}|$ from the atom at $\mathbf{q}$. The ''$\mathbf{q},\mathbf{q}'$'' over the sum in Eq. (6) signifies that only those shells about $\mathbf{q}$ involving periodic images of $\mathbf{q}'$ are considered. The real geometric factors $g_{\mu}(lm,l'm',\hat{\mathbf{d}})$ are

tabulated in the original Slater-Koster paper[1] as well as Table 20-1 of Harrison's book,[8] e.g., $g_\sigma(s,p_x,\hat{\mathbf{d}})=\hat{\mathbf{d}}\cdot\hat{x}$. We take m to designate the customary real linear combinations of spherical harmonics which appear in these tables.

Equations (5) and (6) may be inverted using the orthogonality relations

$$\frac{1}{N}\sum_{\mathbf{k}} e^{i\mathbf{k}\cdot(\mathbf{R}-\mathbf{R}')}=\delta_{\mathbf{R},\mathbf{R}'}, \tag{8}$$

and[28]

$$\sum_{m,m'} g_\mu(lm,l'm',\hat{\mathbf{d}})g_{\mu'}(lm,l'm',\hat{\mathbf{d}})=(2-\delta_{\mu\sigma})\delta_{\mu\mu'}. \tag{9}$$

The first gives

$$\frac{1}{N}\sum_{\mathbf{k}} e^{-i\mathbf{k}\cdot\mathbf{R}}H^{\mathbf{k}}_{\mathbf{q}lm,\mathbf{q}'l'm'} \approx\sum_{\mu} g_\mu(lm,l'm',\widehat{\mathbf{R}+\mathbf{q}'-\mathbf{q}}) \times t_{\tau\tau' ll'\mu}(|\mathbf{R}+\mathbf{q}'-\mathbf{q}|), \tag{10}$$

where the full Hamiltonian may be used since H^0 projects out of the left-hand side for $|\mathbf{R}+\mathbf{q}'-\mathbf{q}|\neq 0$. The nature of the two-center *approximation* is clear from Eq. (10): the $\mu=\sigma,\pi,\ldots$ geometric functions $g_\mu(lm,l'm',\widehat{\mathbf{R}+\mathbf{q}'-\mathbf{q}})$ are in general an incomplete basis for the m,m' dependence of the $\mathbf{q}l,\mathbf{q}'l'$ block of $\Sigma_{\mathbf{k}}e^{-i\mathbf{k}\cdot\mathbf{R}}H^{\mathbf{k}}_{\mathbf{q}lm,\mathbf{q}'l'm'}$. However, since t_μ are by definition coefficients of the existing basis functions, g_μ, the second orthogonality relation gives a precise result for these hopping parameters in spite of the approximate nature of Eqs. (5) and (6),

$$t_{\tau\tau' ll'\mu}(|\mathbf{R}+\mathbf{q}'-\mathbf{q}|)=(2-\delta_{\mu\sigma})^{-1}\frac{1}{N}\sum_{\mathbf{k},m,m'} e^{-i\mathbf{k}\cdot\mathbf{R}} \times g_\mu(lm,l'm',\widehat{\mathbf{R}+\mathbf{q}'-\mathbf{q}}) \times H^{\mathbf{k}}_{\mathbf{q}lm,\mathbf{q}'l'm'}. \tag{11}$$

If Eq. (11) is then formally averaged over the identical results for all z_n neighbors $\mathbf{R}+\mathbf{q}'$ in the same shell, n, about $\mathbf{q}$, one obtains

$$t_{\tau\tau' ll'\mu}(d_n)=[(2-\delta_{\mu\sigma})z_nN]^{-1} \times\sum_{\mathbf{k},m,m'} G^{\mathbf{k}*}_{n\mu}(lm,l'm')H^{\mathbf{k}}_{\mathbf{q}lm,\mathbf{q}'l'm'}, \tag{12}$$

which is the inversion of Eq. (6). Note that here and elsewhere we consider all atoms in a given shell to be equivalent, and therefore assign different values to the shell index n, should $|\mathbf{R}_1+\mathbf{q}_1-\mathbf{q}|=|\mathbf{R}_2+\mathbf{q}_2-\mathbf{q}|$ for two different basis positions $\mathbf{q}_1$ and $\mathbf{q}_2$. Equation (12) is also the result which would be obtained from a least-squares optimization of the agreement in Eqs. (5) and (6) for a given $\mathbf{q}l$, $\mathbf{q}'l'$ block. This equation is particularly useful, since it is still valid if the $\mathbf{k}$ sum is replaced by an appropriately weighted sum over the irreducible wedge of the Brillouin zone. This follows since the matrix dot product $\Sigma_{m,m'}g_\mu(lm,l'm',\hat{\mathbf{d}}_1)g_{\mu'}(lm,l'm',\hat{\mathbf{d}}_2)$ for different directions is a function of $\hat{\mathbf{d}}_1\cdot\hat{\mathbf{d}}_2$, and is therefore invariant under symmetry operations.

B. Site energies and crystal-field parameters

A consistent application of the two-center approximation will admit one-electron potential terms from H in Eq. (2) at sites other than $0\mathbf{q}$. Chadi[16] noted that these crystal-field terms will have the the same kind of expansion as in Eq. (5),

$$H^0_{\mathbf{q}lm,\mathbf{q}'l'm'}\approx\varepsilon_{\tau l}\delta_{ll'}\delta_{mm'} + \sum_{\mathbf{R},\mathbf{q}'}^{\mathbf{R}+\mathbf{q}'\neq\mathbf{q}}\sum_{\mu} g_\mu(lm,l'm',\widehat{\mathbf{R}+\mathbf{q}'-\mathbf{q}}) \times\chi_{\tau ll'\tau'\mu}(|\mathbf{R}+\mathbf{q}'-\mathbf{q}|) \tag{13}$$

$$\approx\varepsilon_{\tau l}\delta_{ll'}\delta_{mm'}+\sum_{n}^{\mathbf{q}}\sum_{\mu} G^0_{n\mu}(lm,l'm') \times\chi_{\tau ll'\tau_n\mu}(d_n). \tag{14}$$

Here $\varepsilon_{\tau l}$ are the orbital site energies, $\chi_{\tau ll'\tau_n\mu}(d_n)$ are the Slater-Koster crystal-field parameters, and the shell sum in Eq. (14) covers all shells of atoms about $\mathbf{q}$. The index order in $\chi_{\tau ll'\tau_n\mu}$ is a reminder that both the l and l' orbitals are at the site of type τ, while the one-electron potential is at the site of type τ_n.

In contrast to the hopping parameter case, the absence of $\mathbf{k}$ dependence in Eqs. (13) and (14) results in an insufficient number of equations to determine the ''bare'' crystal-field parameters, χ, from the Hamiltonian matrix elements for a *single* structure. The number of linearly independent geometric matrices $\mathbf{G}^0_{n\mu}(l,l')\equiv[G^0_{n\mu}(lm,l'm')]$ for all n and μ now determines how many parameters can be determined from the m,m' dependence of each $\mathbf{q}l,\mathbf{q}l'$ block of H^0. It is therefore convenient to rewrite Eq. (14), retaining the largest subset of $G^0_{n\mu}$ in which all members are linearly independent,

$$H^0_{\mathbf{q}lm,\mathbf{q}l'm'}\approx\varepsilon^{\rm eff}_{\tau l}\delta_{ll'}\delta_{mm'} + \sum_{n,\mu\in LI}^{\mathbf{q}} G^0_{n\mu}(lm,l'm')\chi^{\rm eff}_{\tau ll'\tau_n\mu}(d_n), \tag{15}$$

thereby defining effective site energy $\varepsilon^{\rm eff}$ and crystal-field parameters $\chi^{\rm eff}$, which *can* be determined from the matrix elements of H^0. There are, for example, ten such effective parameters for the zinc-blende structure ($\tau=1,2$) treated in an spd basis: six $\varepsilon^{\rm eff}_{\tau l}$ and four crystal-field parameters (one pd and one dd interaction for orbitals of each τ). While the structure of the one-electron Hamiltonian matrix *behaves* as if these were the only crystal-field interactions in the zinc-blende structure, each effective site energy $\varepsilon^{\rm eff}$ and crystal-field interaction $\chi^{\rm eff}$ is a fixed sum, for this structure, over an infinite number of the ''bare'' crystal-field interactions in Eq. (14).

The structure of Eqs. (14) and (15) is complicated by the fact that the matrices $[\delta_{mm'}]$ (for $l=l'$) and $\mathbf{G}^0_{n\mu}(l,l')$, for different μ, are not mutually orthogonal. The orthogonality relation between the g_μ's, Eq. (9), does not carry over to the $G^0_{n\mu}$'s because of the different directions involved in the neighbor sum in Eq. (7). However, there is a transformation which restores this orthogonality if g, G, χ, and $\chi^{\rm eff}$ in Eqs. (13)–(15) are all replaced by the transformed quantities $\widetilde{g}$, $\widetilde{G}$, $\widetilde{\chi}$, and $\widetilde{\chi}^{\rm eff}$, as defined in the Appendix. We denote the transformed counterpart of the μ index by α, so that $\widetilde{\mathbf{G}}^0_{n\alpha}(l,l')\cdot\widetilde{\mathbf{G}}^0_{n'\alpha'}(l,l')\propto\delta_{\alpha\alpha'}$. Moreover, for $l=l'$, the $\alpha=0$ geometric function is now proportional to the identity matrix

$$\widetilde{G}^0_{n0}(lm,lm')=\frac{z_n}{\sqrt{2l+1}}\delta_{mm'}, \tag{16}$$

where z_n is the number of neighbors in shell n. This means that the $\varepsilon_{\tau l}$ and all $\widetilde{\chi}_{\tau l l\tau_n 0}(d_n)$ contribute to the one-electron Hamiltonian in exactly the same way, as coefficients of $\delta_{mm'}$, and can never be unraveled from the matrix elements for a *single* structure. It is convenient to lump all of these contributions into the effective site energies, so that

$$\varepsilon^{\rm eff}_{\tau l}=\frac{1}{(2l+1)N}\sum_{\mathbf{k},m}H^{\mathbf{k}}_{\mathbf{q}lm,\mathbf{q}lm} \tag{17}$$

$$=\varepsilon_{\tau l}+\sum_n^\tau\frac{z_n}{\sqrt{2l+1}}\widetilde{\chi}_{\tau l l\tau_n 0}(d_n) \tag{18}$$

define the effective site energies and their expansions in the bare parameters, respectively.

In terms of the original crystal-field parameters,

$$\widetilde{\chi}_{\tau l l\tau' 0}=\frac{1}{\sqrt{2l+1}}\sum_\mu(2-\delta_{\mu\sigma})\chi_{\tau l l\tau'\mu}\equiv\sqrt{2l+1}\,\chi^{\rm av}_{\tau l l\tau'}, \tag{19}$$

so that

$$\varepsilon^{\rm eff}_{\tau l}=\varepsilon_{\tau l}+\sum_n^\tau z_n\chi^{\rm av}_{\tau l l\tau_n}(d_n), \tag{20}$$

where $\chi^{\rm av}$ may be viewed as the average of $\chi_\mu=\chi_{|\mu|}$ over an extended μ range, $\mu=-l,\ldots,l$.

$\varepsilon^{\rm eff}_{\tau l}$ in Eq. (17) are the usual site energies that would be obtained from fits to band structures or matrix elements for solids if crystal field is ignored, while the $\varepsilon_{\tau l}$ are analogs of isolated-atom site energies. Even though crystal-field interactions may be formally ignored in such fits, $\varepsilon^{\rm eff}_{\tau l}$ are nevertheless intrinsically dependent on local environment,[16,17] which is a reflection of the expansions in Eqs. (18) or (20). When crystal-field interactions are formally included in representations, the ''trace'' definition of the effective site energies in Eq. (17) is the most convenient since (1) the environmental dependence reduces to the simple s-like absence of geometric factors for *all* l as seen in Eqs. (18) or (20), and (2) the remaining crystal-field interactions preserve the trace due to the orthogonality just discussed, e.g., the splittings $\Delta\varepsilon(E_g)$ and $\Delta\varepsilon(T_{2g})$ caused by $\widetilde{\chi}_{dd1}$ (see below) in cubic crystals are such that $2\Delta\varepsilon(E_g)+3\Delta\varepsilon(T_{2g})=0$.

For a crystal with only one equivalent site, and if the l dependence of $\chi^{\rm av}$ in Eq. (20) were ignored, the effect of this equation on the one-electron eigenvalue sum is formally identical for an orthogonal basis to the eigenvalue sum that would be obtained using the bare site energies ε plus a pairwise sum over the ''interatomic potential'' $\chi^{\rm av}(d)$. This is similar to what Cohen and co-workers did by neglecting the pair-potential sum yet using environmental-dependent expressions for their on-site terms in their recent nonorthogonal tight-binding total-energy method.[18] The formal equivalence breaks down for nonorthogonal bases, where band structure shifts also modify the t's, and for two or more inequivalent sites, where the analogy would require expansions about sites of other types besides τ in Eq. (20). Nevertheless, it seems clear that the use of environmentally dependent site energies, especially given their more flexible l-dependent form, may well obviate the need for interatomic potentials.

For the cases $ll'\alpha\neq ll0$, the counterparts of Eqs. (17) and (18) are

$$\sum_{n\in LI}^\tau M_{n'n}\widetilde{\chi}^{\rm eff}_{\tau ll'\tau_n\alpha}(d_n)$$

$$=\frac{1}{N}\sum_{\mathbf{k},m,m'}\widetilde{G}^0_{n'\alpha}(lm,l'm')H^{\mathbf{k}}_{\mathbf{q}lm,\mathbf{q}l'm'} \tag{21}$$

$$=\sum_n^\tau M_{n',n}\widetilde{\chi}_{\tau ll'\tau_n\alpha}(d_n), \tag{22}$$

where, for the given $ll'\alpha$,

$$M_{n'n}=\sum_{m,m'}\widetilde{G}^0_{n'\alpha}(lm,l'm')\widetilde{G}^0_{n\alpha}(lm,l'm'). \tag{23}$$

Here n and n' in Eq. (21) are restricted to the subset of shells for which the $\widetilde{G}^0_{n\alpha}(lm,l'm')$ are linearly independent, i.e., $[M_{n'n}]$ has an inverse. Given the inverse of this structure-dependent matrix, Eq. (21) provides values of the effective crystal-field parameters, while Eq. (22) defines their expansion in the bare parameters for all shells n. It is straightforward to program this treatment, beginning with calculation of the $\widetilde{G}^0_{n\alpha}$ out to some shell cutoff, examination of these matrices for linear independency, and then solution of Eqs. (21)–(23). The virtue of carrying out these calculations in the transformed ''tilde'' basis is decoupling of the α index. Moreover, we found for a variety of structures that the effective crystal-field interactions are the linear combinations in the Appendix. The familiar E_g–T_{2g} splitting of d states in cubic crystals, for example, is due to $\widetilde{\chi}^{\rm eff}_{dd1}$ interactions, i.e., fixed linear combinations of the usual σ, π, and δ crystal-field interactions in the ratios of 3:–4:1, respectively.

The pd crystal-field interaction alluded to above for the cubic diamond and zinc-blende structures considered in this work provides a simple, concrete example. For these structures there is only *one* linearly independent matrix among all the $\widetilde{\mathbf{G}}^0_{n\alpha}(p,d)$ or $\mathbf{G}^0_{n\mu}(p,d)$:

$$G^0_{n\sigma}(pm,dm')=c_nG^0_{1\sigma}(pm,dm'), \tag{24}$$

$$G^0_{n\pi}(pm,dm')=-\frac{2}{\sqrt{3}}c_n G^0_{1\sigma}(pm,dm'), \tag{25}$$

$$\widetilde{G}^0_{n0}(pm,dm')=\sqrt{5/3}c_n G^0_{1\sigma}(pm,dm'), \tag{26}$$

$$\widetilde{G}^0_{n1}(pm,dm')=0, \tag{27}$$

where c_n is a shell-dependent constant, $c_1=1$, which is in fact nonzero only for shells coupling $\mathbf{q}'\neq\mathbf{q}$. The effective interaction is clearly of $\alpha=0$ nature, and if we choose it to be for the first shell, M_{11} of Eq. (23) is 80/9, and Eqs. (21) and (22) become

$$\widetilde{\chi}^{\rm eff}_{\tau pd\tau_1 0}(d_1)=\frac{9}{80\,N}\sum_{\mathbf{k},m,m'}\widetilde{G}^0_{10}(pm,dm')H^{\mathbf{k}}_{\mathbf{q}pm,\mathbf{q}dm'} \tag{28}$$

$$=\sum_n c_n\widetilde{\chi}_{\tau pd\tau_n 0}(d_n). \tag{29}$$

Since $\Sigma_\alpha\widetilde{G}_{1\alpha}\widetilde{\chi}_\alpha=\Sigma_\mu G_{1\mu}\chi_\mu$, one could alternately set $\chi^{\rm eff}_{\tau pd\tau_1\pi}(d_1)=0$, and take this crystal-field interaction to be of standard $pd\sigma$ form, i.e., $\chi^{\rm eff}_{\tau pd\tau_1\sigma}(d_1)=\sqrt{5/3}\widetilde{\chi}^{\rm eff}_{\tau pd\tau_1 0}(d_1)$. Since the transformed crystal-field interactions are not customary, we take the latter approach in reporting our results in this paper.

III. FP-LMTO CALCULATIONS

The FP-LMTO method used here has been described in detail elsewhere.[29,30] While it makes no shape approximation to the one-electron potential, space is divided up into volumes within nonoverlapping muffin-tin spheres plus the encompassing interstitial region for computational convenience. The basis functions are augmented spherical Hankel functions of the form $R_{nl}(r)Y_{lm}(\hat{\mathbf{r}})$, where $R_{nl}(r)$ is a numerical solution of the radial Schrödinger equation inside a given muffin-tin sphere which is matched (value and slope) to a spherical Hankel function outside the sphere. In addition to the usual atomic quantum numbers, these basis functions are characterized by decay energies $-\kappa^2$ of the Hankel-function tails as well as the value of the muffin-tin radius, $R_{\rm MT}$, at which the tail was joined to the numerical solution. Accuracy is insured by the expansion of each atomic orbital in multiple augmented spherical Hankel functions of differing decay energies. In the present work, we have generated self-consistent one-electron potentials and our accurate FP-LMTO band structure using three s basis functions ($-\kappa^2=-0.01$, -1, and -2.3 Ry), three p functions (similarly), and one d function ($-\kappa^2=-0.01$ Ry) for every Si and B atom. The irreducible wedges were sampled with 60 points for both the cubic diamond (cd) and zinc-blende (zb) structures.

The present FP-LMTO method makes use of a separate expansion of the electron *density* in terms of atom-centered and possibly interstitial-sphere-centered augmented spherical Hankel functions to facilitate solution of the Poisson equation.[29,30] We have used 98 functions per site in these expansions, corresponding to two decay energies, $-\kappa^2=-1$ and -3 Ry, and $l_{\rm max}=6$, and included such expansions in interstitial spheres for both cd and zb structures.

The Hamiltonian $\mathbf{H}^{\mathbf{k}}$ and overlap $\mathbf{O}^{\mathbf{k}}$ matrices, which are represented by the Slater-Koster expansions of the previous section, are obtained in separate minimal basis calculations, at 28 points in the irreducible wedge, using the self-consistent one-electron potentials obtained in the multiple-κ calculations described above. In simplest application, each minimal-basis atomic orbital could be taken to be a single augmented spherical Hankel function. In this work, we choose a more accurate representation by using fixed linear combinations of two augmented spherical Hankel functions for each spd atomic orbital. Such linked or contracted bases are common in quantum chemistry calculations, e.g., where contracted sums of Gaussians are used as atomic orbitals. The present linked basis differs from a regular two-κ calculation in that the ratio of coefficients for the two augmented spherical Hankel functions is $\mathbf{k}$ independent. The set of such relative coefficients for the various τl were determined for each phase at its equilibrium volume by minimization of the occupied one-electron eigenvalue sums for the linked, minimal basis, using the fixed self-consistent potentials. The same relative coefficients and κ values were then used for the other two volumes in each case. We also tried choosing these parameters by optimizing the agreement between the minimal-basis and best multiple-κ band structure, as well as the agreement between the Slater-Koster generated band structure and the best band structure. Neither showed significant improvement over the simple one-electron eigenvalue sum minimization.

The asymptotic behavior of especially the overlap hopping parameters $s(d)$ will be governed by the exponential coefficient κ in the Hankel function tails. In order to generate reasonably localized representations, we fixed the decay energy of the most extended Hankel function tail to be $-\kappa_1^2=-0.5$ Ry, which should reduce values of $s(d)$ by roughly two orders of magnitude over a 3.5-Å range. We chose the decay energy for the tail of the second augmented spherical Hankel function in each linked combination to be $-\kappa_2^2\sim-1.5$ Ry. Relative to the $s(d)$'s which would be obtained using just the single κ_1 basis function, we found consistently larger $s(d)$ magnitudes, which also drop off more slowly with distance when using the linked basis. The changes are larger with larger $l+l'$, and for the $s_{ll'\sigma}(d)$, range from 30–60 % increases at the near-neighbor distance to factors of $\sim$2–5 at the fourth-neighbor distance for the s and p parameters of cd Si. That is, on adding the *more localized* κ_2 component, the variational freedom in forming the linked basis has still chosen to form *more extended* minimal basis orbitals. The one-electron bands are, by the way, dramatically improved with the linked basis for the open cd and zb structures.

In general we find some differences between the same overlap functions, $s(d)$, as calculated for different structures and stoichiometries, although for the present fourfold-coordinated phases the agreement is generally $\sim$20% or better. Given the desire for a transferable basis, however, we have performed unitary ''rotations'' of each $\mathbf{k}$-dependent one-electron problem, $(\mathbf{H}^{\mathbf{k}}-\lambda\mathbf{O}^{\mathbf{k}})x=0\rightarrow(\mathbf{H}^{\mathbf{k}}_{\rm rot}-\lambda\mathbf{O}^{\mathbf{k}}_{\rm rot})y=0$, where, suppressing the $\mathbf{k}$ index,

$$\mathbf{H}_{\rm rot}=\mathbf{O}_{\rm rot}^{1/2}\mathbf{O}^{-1/2}\mathbf{H}\mathbf{O}^{-1/2}\mathbf{O}_{\rm rot}^{1/2}. \tag{30}$$

$\mathbf{O}_{\rm rot}^{\mathbf{k}}$, which define these rotations, were calculated from analytic expressions for the complete set of d-dependent functions $s_{\tau\tau' ll' \mu}(d)$, which will be given subsequently. These analytic forms were actually fit to a subset of our directly calculated parameters, so that the $\mathbf{O}_{\rm rot}^{\mathbf{k}}$ and $\mathbf{O}^{\mathbf{k}}$ are not very different. The virtue of this approach is that, without changing the band structure, it provides a perfectly transferable overlap which is exactly represented by two-center expansions, so that issues of nontransferability or non-two-center effects need be addressed only for the Hamiltonian matrices $\mathbf{H}_{\rm rot}^{\mathbf{k}}$. The numerical results presented in this paper will be for these rotated Hamiltonian matrices, and we will therefore make only brief comments on the overlap matrices in Sec. IV.

Finally, as a bookkeeping note, the Hamiltonian and overlap matrices generated routinely by our FP-LMTO code do not correspond to normalized orbitals. Before any other operations, therefore, we apply the same unitary transformation $\Lambda_{\mathbf{q}lm,\mathbf{q}'l'm'}\equiv\delta_{\mathbf{q}\mathbf{q}'}\delta_{ll'}\delta_{mm'}\lambda_{\tau l}$ to both Hamiltonian and overlap matrices for each $\mathbf{k}$, so as to insure normalization. In practice we choose these $\lambda_{\tau l}$ so that the overlap analog of $\varepsilon_{\tau l}^{\rm eff}=1$, since we find the overlap analog of the effective crystal-field interactions to be nearly zero (generally 0.001 or smaller). For comparison, near-neighbor magnitudes of $s_{\tau\tau' ss\sigma}$ are typically in the range 0.3–0.4.

IV. NUMERICAL RESULTS

In this section we present numerical results for the directly calculated tight-binding parameters obtained for the cd phases of Si and B, and zb SiB, each at three different volumes. Comparison is first made between the resultant tight-binding bands and our best multiple-κ band structure, with differences analyzed in terms of the choice of minimal basis orbitals as well as the presence of non-two-center effects. Plots of the calculated hopping parameters, $t_{\tau\tau' ll' \mu}(d)$, are then presented to illustrate general features in both distance and angular momentum dependence, as well as variations over the phases considered. A more practical test of transferability is provided by examining the band structure generated by a single set of analytic functions fit to all of the calculated $t(d)$'s for the set of fourfold-coordinated phases.

A. Band structure

There are two levels of approximation inherent in typical tight-binding band structures. The first is associated with limitations of the particular minimal basis chosen, and the second is the two-center approximation made to the minimal basis matrix elements. These approximations are illustrated by the dotted lines in Figs. 1 and 2, respectively, where the band structure for zb SiB is presented at equilibrium volume. In both cases the solid lines show our most rigorous multiple-κ band structure, provided for comparison, with its Fermi energy taken as the zero of energy. We shall conveniently refer to the lowest four bands, those below the respective gaps (e.g., from $\sim$2 to 3 eV in Fig. 1), as valence bands, and the bands above as conduction bands, even though zb SiB and cd B are metals.

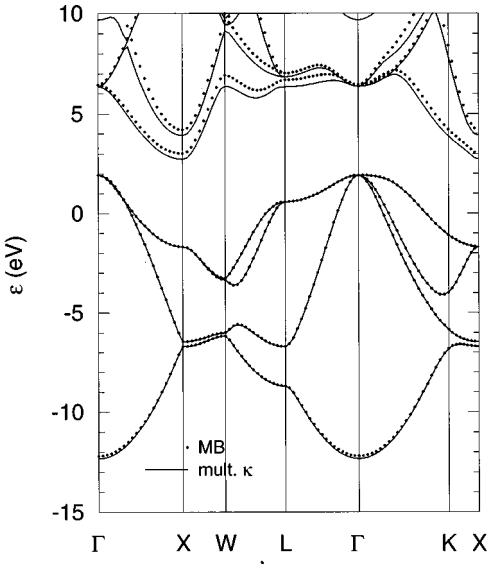

FIG. 1. Comparison of the minimal basis generated band structure (dots) to the best multiple-κ band structure (solid lines) for zb SiB at equilibrium volume. The zero of energy is the latter Fermi energy.

The dotted lines in Fig. 1 show the results of FP-LMTO calculations with a linked, spd minimal basis. The rms difference between these and the mutiple-κ bands is 0.03 eV for the four valence bands, and 0.33 eV for the lowest conduction band, based on a comparison at 145 points throughout the irreducible wedge. The linking coefficients defining this minimal basis were obtained by minimization of the occupied one-electron eigenvalue sum, i.e., states $\varepsilon\leqslant 0$. If this optimization is extended upwards in energy to include the lowest few conduction bands, agreement for the lowest conduction band improves from 0.33 to 0.15 eV, with only a small degradation of the valence-band agreement. The dotted lines in Fig. 2 show the tight-binding bands obtained using parameters calculated from the minimal-basis matrix ele-

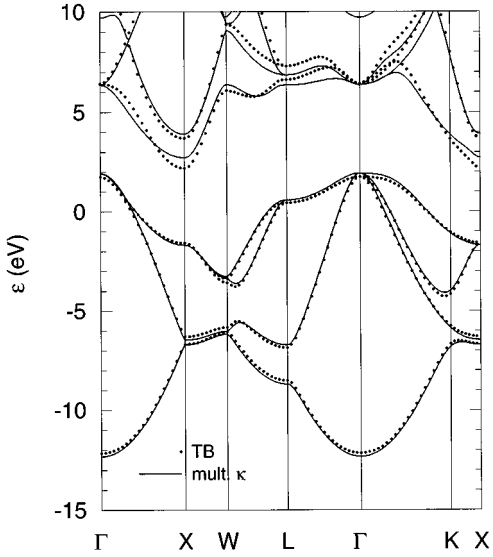

FIG. 2. Comparison of the tight-binding band structure (dots) to the best multiple-κ band structure (solid lines) for zb SiB at equilibrium volume. The zero of energy is the latter Fermi energy.

ments reflected in Fig. 1, and a cutoff of $d_{\max}=1.8a$, where a is the lattice constant. The rms difference between the dotted and solid bands in this figure is 0.10 eV for the four valence bands, and 0.30 eV for the lowest conduction band. The modified linking coefficients just mentioned, while improving the lowest minimal-basis conduction band, actually degrade the corresponding tight-binding comparison from 0.30 to 0.53 eV. We believe this behavior reflects non-two-center effects, as will be discussed below.

It should be emphasized that the tight-binding agreement seen in Fig. 2 can be significantly improved with standard nonlinear minimization of the difference between the two sets of bands. In the case of cd Si, for example, the analog of Fig. 2 exhibits discrepancies of 0.13 and 0.14 for the four valence bands and the lowest conduction band, respectively, and 0.18 eV for all ~ 6 bands up to 4 eV above the valence-band maximum. If the latter rms is minimized by adjusting site energies and selected coefficients of analytic fits to the calculated $t(d_i)$, it can be quickly reduced from 0.18 to 0.03 eV. This demonstrates that our directly calculated parameters are indeed good starting points for such an optimization, and makes contact with previous experience, e.g., a 0.1-eV rms fit to all bands up to 6 eV above the valence-band maximum,[4] obtained with a nonorthogonal sp (versus our spd) basis. Nevertheless, we do not pursue such minimization of band differences in the present work, because it obscures the issue of transferability in that the roles of different parameters are less well defined by the band structure alone in contrast to the matrix elements, effectively band structure plus eigenvectors.

Our tight-binding parameters are calculated directly from the minimal basis matrix elements, and represent the best possible two-center approximation to such matrix elements. A direct comparison of the tight-binding and minimal basis representations is therefore a reflection of non-two-center effects, i.e., an m,m' dependence which cannot be spanned by the two-center geometric factors $g_\mu(lm,l'm',\hat{\mathbf{d}})$, which presumably originate from three-body terms. In the case of the zb SiB band structure, the rms difference between the dotted bands shown in Fig. 1 and those shown in Fig. 2 is 0.10 eV for the four valence bands, and 0.42 eV for the lowest conduction band, again evaluated throughout the irreducible wedge. These finite rms values reflect the extent of non-two-center contributions in the minimal basis matrix elements which we believe is aggravated in the conduction bands by the more itinerant nature[31] of these states in comparison to valence-band states.

We also routinely monitor the differences between tight binding and minimal basis Hamiltonian *matrix* elements, and find these differences to saturate at finite rms values as $d_{\max}$ is increased. In the present zb SiB case, for example, this saturation value for all nonzero matrix elements is 0.24 eV, and is reached for $d_{\max}/a$ in the range 1.42–1.8. If we compare only ss matrix elements, however, the rms difference becomes arbitrarily small with increasing $d_{\max}$, reflecting the fact that the two-center approximation impacts only those degrees of freedom associated with multiple values of the magnetic quantum number m, as can be seen from Eq. (10). The saturation rms value for the matrix element comparison also becomes smaller for the full set of spd matrix elements if a more localized basis is used, e.g., it is 0.08 eV for the one-κ basis, $\kappa^2=0.5$ Ry, discussed in Sec. III. This is consistent with the intuitive expectation that a more localized basis should reduce the importance of three-center terms. Unfortunately, while there is much improved agreement between minimal-basis and tight-binding band structures for this more localized one-κ basis, both are in poor agreement with our accurate multiple-κ result.

The converse effect, a more extended basis, is illustrated by the zb SiB modified linking coefficients mentioned above, which improved the lowest minimal-basis conduction band but made the corresponding tight-binding band worse. That modification generally increased the magnitudes of both $s(d)$ and $t(d)$ parameters for $ll'=ld$, which persisted for the rotated $t(d)$'s corresponding to the transferable overlap functions. These ld parameters are not on the whole larger than, e.g., the pp parameters, indicating that an extended basis is a necessary but not sufficient condition for significant three-body effects. Harrison's bond orbital treatment, for example, suggests that the directionality of sp^3 hybrids may allow an explicit two-center treatment for quite extended orbitals.[8]

As discussed in Sec. II B, the zb and cd structures may be characterized by two effective crystal-field interactions per site for an spd basis, one pd and one dd interaction, discounting those other crystal-field interactions which couple to and are intrinsic parts of the effective site energies. Both effective pd and dd interaction parameters have been calculated from the minimal-basis matrix elements, and their effects are incorporated into the tight-binding bands in Fig. 2. The latter, although not small, has negligible impact on the valence and first few conduction bands, and we shall ignore it. The former, which may be conveniently treated as effective near-neighbor σ interactions, $\chi_{SipdB\sigma}(d_1)$ and $\chi_{BpdSi\sigma}(d_1)$, are responsible for a ~ 1-eV shift in the lowest conduction band throughout the Brillouin zone. If these interactions were removed from the tight-binding bands in Fig. 2, the lowest conduction band would drop by 1.04 and 1.08 eV at Γ and X, respectively, while the highest valence band would move upward by 0.36 and 0.01 eV, similarly. We obtain very similar results for cd Si. In other words, the cubic diamond phase of Si would be a metal were it not for pd crystal-field interactions. To be more precise, an sp basis typically does give an insulating gap for cd Si. When adding d states, the overall effect of the new hybridization interactions (t's) is to lower the lowest conduction band, which is offset by the pd crystal-field interactions tending to raise this band.

B. Parameters

Figure 3 shows our directly calculated Si-Si hopping interactions for s and p angular momenta. The figure includes results for Si-Si interactions in both cd Si (closed circles) and in zb SiB (open circles), and for three volumes each ($V/V_0=0.8$, 1, and 1.2) so that the points for each shell appear in triples. The roughly exponential behavior seen at the larger separations persists as far as we have calculated, $d=11$ Å, at which point the largest parameters are less than 3×10^{-4} eV in size. The curves are fits, and the rms percentage scatter about them is 5% or less considering 15 points at $d<5$ Å.

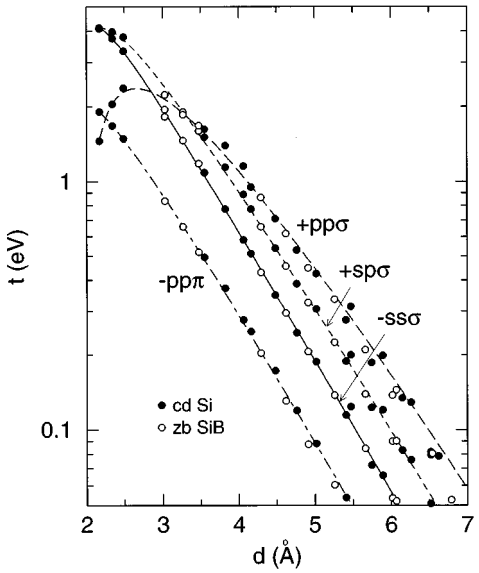

FIG. 3. Calculated Si-Si Hamiltonian Slater-Koster parameters, $t_{ll'\mu}(d)$, for s and p angular momentum. Results are shown for Si-Si interactions in cd Si and zb SiB. The designation, e.g., ''$-pp\pi$'' signifies that $-t_{pp\pi}(d)$ is plotted. The curves are fits as tabulated in Table II.

The corresponding scatter is larger for ld interactions, although generally less than $\sim$20%, except for the $dd\sigma$ case at 32%, which may be seen in Fig. 4. In all cases the actual rms differences for this same range are $\leqslant$0.1 eV. Note that these parameters, a subset of which were used to generate Fig. 2, are calculated from the matrix elements of our rotated Hamiltonians (see Sec. III) so that the corresponding overlap parameters are perfectly transferable and smooth by construction.

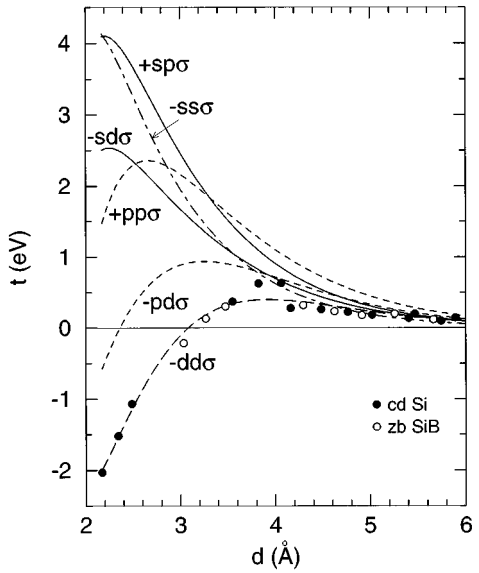

FIG. 4. Si-Si Hamiltonian Slater-Koster parameters $t_{ll'\sigma}(d)$ for all σ interactions. Calculated results are shown for the Si-Si $dd\sigma$ interaction in cd Si and zb SiB. The curves are fits to these and similarly calculated results (not shown), and are tabulated in Table II. The designation, e.g., ''$-pd\sigma$,'' signifies that $-t_{pd\sigma}(d)$ is plotted.

Many of the Slater-Koster parameters must change sign or approach 0 at small d due to the nodal structure of the orbitals. This is easily understood for the overlap parameters from simple orbital sketches, e.g., $s_{pp\sigma}(d)$ should be negative at large separations, yet approach the normalization 1 as $d\rightarrow 0$. As a manifestation of these trends, we find many of the overlap parameters in the present work to bend over at the smaller values of d, similar to the $t_{pp\sigma}$ curve in Fig. 3. This behavior is quite systematic, e.g., it is absent in $s_{ss\sigma}(d)$, and increases with $l+l'$ for the other σ parameters, $s_{ll'\sigma}(d)$. In all cases, however, these overlap parameters retain the same sign throughout the range investigated in this work ($2.17<d<11$ Å for Si-Si interactions).

The situation for the Hamiltonian parameters is similar, although more dramatic, as seen in Fig. 4, where all σ interactions are shown. The increasing effect with $l+l'$ may be understood because the orbitals for larger l are both more extended due to higher site energies in the present materials, but also because of narrower lobes which poke out farther in the bond direction for the σ interactions, and therefore cross nodal planes of opposing orbitals at larger separation. The quantities plotted in Fig. 4, $\pm t$, have been chosen so that parameters with the ''correct'' sign are positive, and similarly in Fig. 3. Thus it can be seen that the Si-Si near-neighbor $t_{dd\sigma}$ have the wrong sign because of the effect just discussed. This may not be generally true, since for a nonorthogonal basis, the Hamiltonian Slater-Koster parameters depend on the energy zero, i.e., an overall shift by $\Delta\varepsilon$ of the band-structure as a whole changes $t(d)$ to $t(d)+\Delta\varepsilon s(d)$. Nevertheless, we find the ratios $-t(d)/s(d)$ to be relatively flat (independent of d) for the $ss\sigma$ cases, and increasingly more negative and more down-turned at small d for the larger values of $l+l'$. Thus a general conclusion for σ interactions appears to be a general tendency for the $s(d)$ to bend over at small d, more so for larger $l+l'$, and that similar but *more pronounced* effects occur for the $t(d)$.

The sp subset of our calculated near-neighbor Slater-Koster parameters for cd Si at equilibrium volume are compared in Table I to results from two different band-structure fits using sp bases.[4,6] The agreement is on the whole quite good, with our larger $t_{sp\sigma}$ and $t_{pp\pi}$ magnitudes being the most noticeable differences out of the range of the previous work. If the cd Si band structure is calculated with just the sp subset of our nonorthogonal parameters, the agreement with the full spd calculation is excellent for the lower half of the valence band, and the most noticeable difference for the top half is the sp Γ point which is 0.8 eV higher than the corresponding spd value. The lowest conduction-band states are fairly close at Γ; however, the sp band is significantly higher (3.8 eV) at X than the spd result, and similarly at other zone face states. It is the d-state hybridization which pushes the lowest conduction band down at these points, and we suspect that the smaller $t_{sp\sigma}$ and $t_{pp\pi}$ seen for Refs. 4 and 6 are required to achieve the same effect within an sp basis.

Our parameters fall off more slowly than do those in Refs. 4 and 6, where interactions through third neighbors were sufficient to represent the band structure of cd Si. Our tight-binding band structure for cd Si at $V=V_0$ is fully converged by $d_{\max}=1.42\,a$, or eight distinct neighbor distances, with an rms difference from our best multiple-κ bands of 0.18 eV for

TABLE I. Comparison of near-neighbor ($d=2.351$ Å) Slater-Koster parameters for cd Si at the experimental equilibrium volume. The overlap parameters s are dimensionless; the Hamiltonian parameters t are in eV. The present parameters are a subset of the full spd representation, whereas the others are from sp representations.

	$s_{ss\sigma}$	$s_{sp\sigma}$	$s_{pp\sigma}$	$s_{pp\pi}$	$t_{ss\sigma}$	$t_{sp\sigma}$	$t_{pp\sigma}$	$t_{pp\pi}$
present	0.2700	−0.3603	−0.3590	0.2074	−3.7423	3.9797	2.0430	−1.6754
Ref. 4	0.2705	−0.3426	−0.3755	0.2614	−3.2766	3.2668	1.9548	−1.0335
Ref. 6	0.3036	−0.3743	−0.2455	0.1307	−3.6463	2.7103	2.1462	−1.3319

states up to 4 eV above the valence-band top. This discrepancy increases to 0.24 and 0.31 eV for five and three neighbor distance cutoffs, respectively. The zb SiB tight-binding bands are also essentially converged by $d_{\max}=1.42\,a$ at $V=V_0$, although the rms discrepancy in this case increases from 0.13 to 0.34 eV at the five-neighbor-distance cutoff. We have not yet systematically explored variation of the decay energies of the augmented spherical Hankel function tails as a way of creating more localized bases; however, we noted that optimization of our linked minimal basis (two such functions per atomic orbital with fixed relative coefficients) had the opposite effect by creating more *extended* orbitals than either of the two-component augmented Hankel functions, while simultaneously greatly improving the band structure. Although interactions through third neighbors are sufficient to represent the band structure alone for cd Si,[4,6] it is not yet clear whether the same is also true for the more challenging case of matrix elements as confronted in this work. Sanchez-Portal, Artacho, and Soler[24] have applied projection techniques to *ab initio* plane-wave calculations for cd Si in order to obtain matrix elements in atomic orbital bases. While they found a standard atomic basis (sp, STO-4G) to yield a fully converged band structure for interactions through only third neighbors, they obtain both better band structure and more complete coverage of the Hilbert space of occupied plane-wave eigenfunctions with a ''scaled'' atomic basis, which they note usually requires ''a longer range of interactions.''

Beyond comparing the parameters themselves as in Fig. 3, a more practical test of transferability is to see how well a single fixed set of $s(d)$, $t(d)$ functions performs. To this end, Table II provides analytic fits to our calculated Slater-Koster hopping parameters t, for all of the fourfold-coordinated phases considered in this work. The functional form is

$$t(d)=A_1 d^{B_1} e^{-C_1 d}+A_2 d^{B_2} e^{-C_2 d}, \tag{31}$$

where the exponents $C_1=0.7/a_0$ and $C_2=1.2/a_0$ for all parameters, and a_0 is the Bohr radius. These choices of C_1 and C_2 were motivated by the decay energies used for the two augmented spherical Hankel functions in the linked basis. The same functional form was used to represent our perfectly transferable (by construction) overlap parameters, i.e., the $s(d)$ functions used to assemble the matrices $\mathbf{O}^{\mathbf{k}}_{\rm rot}$ of Eq. (30). Recall that all t's cited and used in this paper were obtained from the $\mathbf{H}^{\mathbf{k}}_{\rm rot}$ matrices defined by this equation. The coefficients describing these analytic $s(d)$ functions are also given in Table II.

To complete the representation of the bands, Table III gives the effective site energies and pd crystal-field terms. These are individually tabulated for the different structures and volumes, as it is beyond the scope of the present paper to generate structurally dependent fits to these quantities. The known structure-dependent expansions given by Eqs. (18) and (29), however, provide the means for obtaining such fits, by varying parametrized analytic forms for the d dependence of the bare crystal-field interactions so as to optimize the agreement in these equations. We are currently exploring such fits for a broader class of structures than discussed here, as well as the use of prior structure-dependent shifts of the bands so as to insure that the one-electron eigenvalue sum alone would reproduce the total energies.[18] As noted earlier, such shifts modify the t's, and so we are also investigating possible representations of the differences $\Delta t_{\tau\tau' ll'\mu} \equiv t_{\tau\tau' ll'\mu}-(\varepsilon_{\tau l}+\varepsilon_{\tau' l'})s_{\tau\tau' ll'\mu}/2$, which would be invariant under uniform shifts of the band structure, rather than of the t's themselves.

C. Transferability

Nonorthogonal bases are generally expected to yield more transferable tight-binding parameters than orthogonal bases. While our results are consistent with this expectation, they also raise the possibility that nonorthogonal hopping parameters which accurately describe the best local-density band structure and matrix elements may not be widely transferable, without, for example, special environment-dependent representational procedures as are now being applied in the orthogonal case.[14] We are currently investigating this issue for a wider class of structures than the fourfold-coordinated phases considered in this work, and briefly mention some preliminary results for other structures here in regard to the issue of transferability.

For both the fcc phase of Si (12-fold coordination) and the $B2$ or CsCl phase of SiB (eightfold coordination), we find magnitudes of the nonorthogonal hopping parameters, $t(d)$, which are 10–30 % larger than would be indicated by the fits to the fourfold coordinated t's given in Table II, considering the sp parameter subset over the first five-neighbor distances. As throughout this paper, these $t(d)$'s were obtained using Eq. (30) and therefore correspond to our standard transferable overlap parameters, $s(d)$, which are also given in Table II. The effect on the band structure from using the smaller $t(d)$'s in the table is to give systematically narrower bands by 20–25 % over those obtained with the directly calculated t's. The rms discrepancies with our best multiple-κ band structure for states up to 4 eV above the Fermi level are consequently poor, over 1 eV, as may be seen in the ''Table II t's'' column of Table IV for fcc Si and $B2$ SiB. We also removed an atom from the eight-atom cd Si cell, and relaxed

TABLE II. Analytic fits to calculated Slater-Koster parameters for the fourfold-coordinated Si/B phases. In the name, ''1'' designates Si, and ''2'' B. The fits are of the form $s,t=A_1d^{B_1}e^{-C_1d}+A_2d^{B_2}e^{-C_2d}$, where the superscripts O and H designate s (dimensionless) and t (eV), respectively, for d in Å. The coefficients $C_1=0.7/a_0=1.322\ 81$ and $C_2=1.2/a_0=2.267\ 67$, for all parameters, where a_0 is the Bohr radius. These fits correspond to the rotated matrices discussed below Eq. (30).

Name	A_1^O	B_1^O	A_2^O	B_2^O	A_1^H	B_1^H	A_2^H	B_2^H
$11ss\sigma$	20.630 48	−0.40	−31.874 59	1.07	−54.906 97	0.59	6000.155 61	−5.20
$11sp\sigma$	−6.036 11	0.63	34.644 12	−0.60	42.247 67	1.05	−2911.813 92	−3.60
$11sd\sigma$	4.140 61	0.78	−345.478 32	−3.60	−17.090 16	1.51	4740.042 16	−5.20
$11pp\sigma$	−5.740 14	1.00	31.373 57	0.54	19.528 64	1.77	−479.683 76	−0.24
$11pp\pi$	8.233 39	−0.37	−57.547 91	−1.79	−24.482 35	0.62	184.023 52	−1.80
$11pd\sigma$	3.697 03	1.20	−26.680 44	0.74	−31.738 09	1.38	138.769 77	2.26
$11pd\pi$	−9.897 65	−0.23	279.829 99	−3.20	90.788 49	0.20	−146.385 30	1.89
$11dd\sigma$	8.878 96	0.70	−21.636 44	1.99	−124.032 81	0.55	248.562 39	2.52
$11dd\pi$	−8.258 32	0.17	415.955 15	−3.40	388.578 22	−0.37	−695.119 30	1.61
$11dd\delta$	2696.721 19	−4.75	−4956.758 27	−2.94	−195.317 70	−0.71	212.242 36	1.71
$12ss\sigma$	4.652 94	0.39	−13.643 77	−1.01	−59.576 07	0.42	514.291 41	−2.20
$12sp\sigma$	−6.126 98	0.40	14.508 34	0.41	41.025 12	0.82	−696.010 09	−2.40
$12ps\sigma$	−7.382 25	0.44	15.916 17	0.73	38.875 40	1.03	−377.585 70	−1.60
$12sd\sigma$	10.274 62	0.12	−26.038 82	0.86	−27.537 39	1.03	494.406 77	−1.06
$12ds\sigma$	9.692 42	0.20	−22.647 42	1.01	−23.122 99	1.26	200.637 99	−0.60
$12pp\sigma$	−10.458 97	0.40	28.394 55	1.09	18.989 91	1.59	−339.432 59	−0.55
$12pp\pi$	7.930 25	−0.58	−15.424 94	−0.26	−88.463 20	−0.40	212.541 69	0.31
$12pd\sigma$	16.485 64	0.16	−44.394 39	1.26	−4.890 33	2.39	168.458 33	0.95
$12pd\pi$	−1.324 28	0.60	−2.514 35	2.77	180.469 47	−0.46	−531.495 31	0.60
$12dp\sigma$	11.809 09	0.25	−33.176 81	1.18	−7.991 19	2.01	161.940 54	0.62
$12dp\pi$	−0.557 03	1.00	−3.916 10	2.44	167.353 02	−0.52	−423.304 45	0.57
$12dd\sigma$	−2.154 13	−0.80	0.568 46	5.02	−34.405 45	1.46	94.934 72	3.23
$12dd\pi$	−39.455 69	−0.92	93.566 19	0.19	478.845 85	−0.71	−1203.102 43	0.85
$12dd\delta$	77.879 93	−2.60	−165.338 30	−1.27	125.554 86	−5.20	−1.928 00	4.40
$22ss\sigma$	3.570 88	0.42	−7.873 29	−2.20	−41.748 99	0.65	176.337 57	−2.80
$22sp\sigma$	−3.729 62	0.57	7.307 29	−0.40	29.872 12	1.01	−251.195 84	−2.89
$22sd\sigma$	6.75536	0.26	−15.23737	0.84	94.53670	−5.20	−6.870 10	4.65
$22pp\sigma$	−3.678 31	0.74	11.498 99	0.20	22.854 34	1.27	−171.877 51	−0.40
$22pp\pi$	3.496 80	−0.37	−7.664 09	−2.40	−37.952 18	−0.11	59.117 86	0.17
$22pd\sigma$	5.011 70	0.60	−16.760 47	0.90	−23.798 58	1.17	143.508 47	1.39
$22pd\pi$	−7.216 72	−0.43	14.418 23	−0.48	−35.567 10	−4.00	5.886 21	4.23
$22dd\sigma$	15.828 33	0.00	−39.458 87	1.25	−308.309 24	−0.40	619.911 57	1.57
$22dd\pi$	−25.350 85	−0.80	63.020 06	0.10	−77.617 05	0.03	13.102 70	4.44
$22dd\delta$	22.603 67	−1.99	−49.087 00	−1.07	26.453 01	−0.39	−11.000 90	3.39

both the internal parameter and atomic volume to obtain a mixed threefold- and fourfold-coordinated Si_7-vacancy phase. The corresponding rms discrepancy in this case is better, 0.55 eV, which is still not particularly good, although a constant shift of the bands would reduce this discrepancy to 0.35 eV. Our directly calculated $t(d)$'s, by contrast, give about the same 0.1–0.2-eV rms discrepancy for *all* phases we have considered, as may be seen in the ''calc t's'' column in Table IV. Note that for all of the results cited in Table IV we have used our calculated, structure-dependent site energies and crystal-field terms. These are tabulated in Table III for the fourfold coordinated phases, except for the dd crystal-field interactions, which have little impact in this energy range. Since the Table II t's are of less use for the other coordinations, we have not given the corresponding site energies and crystal-field parameters in those cases.

The implications of Table IV are that the fixed $t(d)$ functions given in Table II do reasonably well for chemical and atomic-volume variation, but not for change in coordination. While suggestive, we feel it would be premature to make this a general conclusion about *ab initio* calculated t's since our parameters are a direct reflection of our choice of minimal basis atomic orbitals, and it remains to be seen whether other choices can give comparable representation of the matrix elements and band structure, and how that degree of freedom impacts transferability. Moreover, even if there is coordination dependence of the hopping parameters, more sophisticated environment-dependent analytic forms[14] should still permit fully transferable representations. These are subjects of future investigation, along with finding shorter-ranged representations, and we emphasize that the major point of the present paper is the method of calculating *ab initio* param-

TABLE III. Effective site energies $\varepsilon_l^{\rm eff}$ and near-neighbor $pd\sigma$ crystal-field interactions $\chi_{pd\sigma}^{\rm eff}$ in eV, for different sites in the phases considered in this work. The latter are more precisely written $\chi_{\tau pd\tau_1\sigma}^{\rm eff}(d_1)$, and are listed according to the site τ where the orbitals are located, while τ_1 is the near-neighbor atom type. V_0 is the theoretical equilibrium volume corresponding to lattice constants of 5.408, 4.624, and 4.014 Å for cd Si, zb SiB, and cd B, respectively.

Phase	V/V_0	site	$\varepsilon_s^{\rm eff}$	$\varepsilon_p^{\rm eff}$	$\varepsilon_d^{\rm eff}$	$\chi_{pd\sigma}^{\rm eff}$
cd Si	0.8	Si	−7.573	−2.256	7.426	−1.574
cd Si	1.0	Si	−8.673	−2.952	6.467	−1.383
cd Si	1.2	Si	−9.180	−3.238	6.196	−1.169
zb SiB	0.8	Si	−7.293	−1.707	8.290	−1.408
zb SiB	1.0	Si	−8.207	−2.187	7.996	−1.313
zb SiB	1.2	Si	−8.735	−2.516	7.694	−1.171
zb SiB	0.8	B	−5.846	−0.963	14.116	−1.770
zb SiB	1.0	B	−7.136	−1.649	13.782	−1.758
zb SiB	1.2	B	−7.772	−2.070	13.847	−1.634
cd B	0.8	B	−6.908	−1.136	15.850	−1.841
cd B	1.0	B	−8.017	−1.829	15.601	−1.701
cd B	1.2	B	−8.558	−2.266	15.896	−1.536

eters whose success for *all* phases is demonstrated by the ''calc t's'' column in Table IV.

We find the transferability between close-packed and fourfold-coordinated phases to be significantly worse for orthogonal bases, with occasional differences in the $t^{or}(d)$'s up to a factor of 2. In reverse of the nonorthogonal case, we find the close-packed $t^{or}(d)$'s to be smaller in magnitude than the open-packed values, consistent with recent observations.[14] Unfortunately, we find that Löwdin orthogonalization[32] also amplifies non-two-center contributions in the resultant orthogonal Hamiltonian matrices, so that our directly calculated orthogonal-basis, two-center tight-binding parameters give poorer representation of the band structure. We obtain better orthogonal basis tight-binding band structures by carrying out Löwdin orthogonalization using the two-center approximate Hamiltonian and overlap matrices. This area is also under ongoing investigation.

TABLE IV. The rms agreement between tight-binding and accurate multiple-κ band structure for states up to 4 eV above the Fermi level. Our directly calculated t's (''calc t's'') do reasonably well for *all* coordinations (z); however, these t's display some coordination dependence, so that a fit to just the values for fourfold-coordinated phases (''Table II t's'') does not give accurate band structure at other coordinations. All tight-binding calculations use the s's in Table II. Tight-binding cutoffs have been chosen to insure convergence of the rms values to ~0.01 eV or better. Lattice constants a correspond to theoretical equilibrium volumes for the middle cd Si and all other phases. Irreducible wedges were sampled with 145 (cd, zb, fcc) and 120 ($B2$, Si_7vac) points.

Phase	a (Å)	z	rms (eV) calc t's	rms (eV) Table II t's
cd Si	5.020	4	0.20	0.25
cd Si	5.408	4	0.18	0.18
cd Si	5.747	4	0.19	0.16
zb SiB	4.624	4	0.12	0.18
cd B	4.014	4	0.10	0.12
Si_7vac[a]	5.134	3,4	0.18	0.55
$B2$ SiB	2.687	8	0.08	1.32
fcc Si	3.832	12	0.14	1.25

[a]Space group $P\bar{4}3m$, Si atoms at $3c$ and $4e$ ($x=0.224$) sites.

V. SUMMARY

We have derived relatively simple analytic expressions which define two-center Slater-Koster hopping parameters, effective site energies, and effective crystal-field parameters in terms of **k**-dependent Hamiltonian matrix elements in any localized minimal basis, and analogous quantities for the overlap. While directly applicable to band-structure methods formulated in localized bases, these expressions could also be used, for example, by plane-wave-based calculations which have been projected onto atomic-orbital bases.[24]

We have shown that a natural transformation of the crystal field parameters isolates that subset of these interactions which couples to the site energies, creating structure-dependent effective site energies $\varepsilon^{\rm eff}$, which are in fact the usual site energies that would be extracted from fits to the band structure of a single structure. Expansions of $\varepsilon^{\rm eff}$ in terms of the bare crystal-field interactions resemble interatomic potential sums, providing some support for the use of environment-dependent site energies in place of interatomic potentials in recent tight-binding total-energy representations.[18]

Our calculated parameters provide the *best possible* two center representation of the Hamiltonian or overlap matrix elements, automatically projecting out the best two center approximations to three-center terms. Residual differences between the minimal basis matrix elements and those reconstructed from the tight-binding parameters therefore provide a quantitative measure of non-two-center effects for a given basis and material.

We have used the expressions derived in this work to calculate spd, nonorthogonal tight-binding parameters in the two-center approximation for fourfold-coordinated phases of Si, SiB, and B, at three volumes each. The *ab initio* matrix elements were generated with a linked minimal basis using the FP-LMTO method. Compared to our best FP-LMTO band structure, we obtain good tight-binding valence bands (0.10–0.13-eV rms), with the lowest conduction band treated less well (0.14–0.30 eV) due to larger intrinsic non-two-center contributions in the corresponding FP-LMTO minimal basis matrix elements. We were able to quickly improve rms values for cd Si by a factor of ~5 using standard nonlinear minimization of the differences between the band structures, showing that our directly calculated parameters are indeed good starting points for such optimization. However, fits to band structure alone are underconstrained in comparison to representations of the matrix elements, effectively band structure plus eigenvectors, and therefore compromise the distinctions between two-center and non-two-center contributions as well as between different parameters. While this may be advantageous in obtaining a smaller set of effective parameters for a given structure, it will ultimately obscure the issue of transferability especially for complex, multicomponent systems.

A few test cases of higher and lower coordination have also been considered. While our directly calculated Slater-Koster parameters provide roughly equally good representation of the matrix elements and band structure for *all* phases considered, a single set of analytic hopping parameter functions fit to the fourfold-coordinated values appears to be relatively transferable over chemical and atomic-volume variation, though, not over change in coordination. Transferable representation of *ab initio* calculated parameters may therefore require environment-dependent features, as have been considered in the orthogonal case.[14]

ACKNOWLEDGMENTS

This work was performed under the auspices of the U.S. Department of Energy by Lawrence Livermore National Laboratory under Contract No. W-7405-Eng-48. We are grateful to M. van Schilfgaarde for providing a new version of the FP-LMTO codes which was used in carrying out the linked basis calculations described here.

APPENDIX

There is a unique transformation of the crystal-field parameters and the associated geometric factors

$$\tilde{\chi}_{ll'\alpha}=\sum_{\mu} T_{\alpha\mu}(ll')\chi_{ll'\mu}, \tag{A1}$$

$$\tilde{g}_{\alpha}(lm,l'm',\hat{\mathbf{d}})=\sum_{\mu} g_{\mu}(lm,l'm',\hat{\mathbf{d}})[T^{-1}(ll')]_{\mu\alpha}, \tag{A2}$$

which isolates those crystal-field contributions $\tilde{\chi}_{ll0}$ which couple to the site energies, and which restores orthogonality of the matrix dot product

$$\sum_{m,m'} \tilde{g}_{\alpha}(lm,l'm',\hat{\mathbf{d}}_1)\tilde{g}_{\beta}(lm,l'm',\hat{\mathbf{d}}_2)=\delta_{\alpha\beta}f_{ll'\alpha}(\hat{\mathbf{d}}_1\cdot\hat{\mathbf{d}}_2), \tag{A3}$$

when the directions $\hat{\mathbf{d}}_1$ and $\hat{\mathbf{d}}_2$ are different. Here $f_{ll'\alpha}(x)$ is a polynomial in x with $f_{ll'\alpha}(1)=1$. Note that the two-center expansion is preserved by construction, $\Sigma_{\alpha}\tilde{g}_{\alpha}\tilde{\chi}_{\alpha}=\Sigma_{\mu}g_{\mu}\chi_{\mu}$, and that we have suppressed type and shell designations in the crystal-field parameters. If $\tilde{G}^{0}_{n\alpha}(lm,l'm')$ are defined in terms of the $\tilde{g}_{\alpha}(lm,l'm',\hat{\mathbf{d}})$ according to Eq. (7), then the orthogonality

$$\sum_{m,m'} \tilde{G}^{0}_{n\alpha}(lm,l'm')\tilde{G}^{0}_{n'\beta}(lm,l'm')\propto\delta_{\alpha\beta} \tag{A4}$$

follows from Eq. (A3).

For $l\leq l'\leq d$, the transformation is

$$\tilde{\chi}_{pp0}=(\chi_{pp\sigma}+2\,\chi_{pp\pi})/\sqrt{3},$$

$$\tilde{\chi}_{pp1}=(\chi_{pp\sigma}-\chi_{pp\pi})\sqrt{2/3},$$

$$\tilde{\chi}_{pd0}=(\sqrt{3}\chi_{pd\sigma}-2\,\chi_{pd\pi})/\sqrt{5},$$

$$\tilde{\chi}_{pd1}=(\chi_{pd\sigma}+\sqrt{3}\chi_{pd\pi})\sqrt{2/5},$$

$$\tilde{\chi}_{dd0}=(\chi_{dd\sigma}+2\,\chi_{dd\pi}+2\,\chi_{dd\delta})/\sqrt{5},$$

$$\tilde{\chi}_{dd1}=(3\,\chi_{dd\sigma}-4\,\chi_{dd\pi}+\chi_{dd\delta})\sqrt{2/35},$$

$$\tilde{\chi}_{dd2}=(\chi_{dd\sigma}+\chi_{dd\pi}-2\,\chi_{dd\delta})\sqrt{2/7}. \tag{A5}$$

These would be orthogonal combinations for each ll', if considered over the full $\mu=-l,\ldots,l$ range ($\chi_{\mu}=\chi_{|\mu|}$), for example, $(1,1,1)/\sqrt{3}$ and $(-1,2,-1)/\sqrt{6}$ for $ll'=pp$. Using the abbreviation $g_{ll'\mu}=g_{\mu}(lm,l'm',\hat{\mathbf{d}})$, and similarly for the $\tilde{g}$, the inverse transformations are

$$\tilde{g}_{pp0}=(g_{pp\sigma}+g_{pp\pi})/\sqrt{3},$$

$$\tilde{g}_{pp1}=(2g_{pp\sigma}-g_{pp\pi})/\sqrt{6},$$

$$\tilde{g}_{pd0}=(\sqrt{3}g_{pd\sigma}-g_{pd\pi})/\sqrt{5},$$

$$\tilde{g}_{pd1}=(2g_{pd\sigma}+\sqrt{3}g_{pd\pi})/\sqrt{10},$$

$$\tilde{g}_{dd0}=(g_{dd\sigma}+g_{dd\pi}+g_{dd\delta})/\sqrt{5},$$

$$\tilde{g}_{dd1}=(6g_{dd\sigma}-4g_{dd\pi}+g_{dd\delta})/\sqrt{70},$$

$$\tilde{g}_{dd2}=(2g_{dd\sigma}+g_{dd\pi}-2g_{dd\delta})/\sqrt{14}. \tag{A6}$$

Note that in matrix form, and for each ll', $\mathbf{T}$ should act from the left on column vector $[\chi_{\mu}]$, while $\mathbf{T}^{-1}$ should act from the right on row vector $[g_{\mu}]$, thus insuring $\Sigma_{\alpha}\tilde{g}_{\alpha}\tilde{\chi}_{\alpha}=\Sigma_{\mu}g_{\mu}\chi_{\mu}$. In regard to the matrix dot products, e.g., Eq. (A3), but for the same directions, $\hat{\mathbf{d}}_1=\hat{\mathbf{d}}_2$, the g_{μ} are orthogonal in the μ index with normalizations $2-\delta_{\mu\sigma}$, while the $\tilde{g}_{\alpha}$ defined by Eqs. (A6) are orthonormal in the α index. Note also that $\tilde{g}_{0}(lm,lm',\hat{\mathbf{d}})=\delta_{mm'}/\sqrt{2l+1}$.

The orthogonality relations Eqs. (9) and (A3) for the g_{μ} and $\tilde{g}_{\alpha}$, respectively, are ultimately properties of the rotation group matrices for different angular momentum.[33] Transforming these expressions to correspond to the customary real orbitals is cumbersome, so that we have verified the orthogonality relations directly from the tabulated Slater-Koster geometric functions as in Table 20-1 of Harrison's book.[8] To review the notation, our geometric function $g_{\sigma}(p_x,d_{xy},\hat{\mathbf{d}})=\sqrt{3}l^2m$, for example, which is the coefficient of Harrison's $V_{pd\sigma}$ in his expression for $E_{x,xy}$, where Harrison (and we only in this sentence) uses l,m,n to designate the direction cosines defining $\hat{\mathbf{d}}=(l,m,n)$.

The orthogonality relations may be proved as follows. First, construct column vectors $L(\hat{\mathbf{d}})$ from the m dependence of $g_{\sigma}(lm,s,\hat{\mathbf{d}})$ and note that the matrices $\mathbf{g}_{\sigma}(l,l',\hat{\mathbf{d}})=[g_{\sigma}(lm,l'm',\hat{\mathbf{d}})]=L(\hat{\mathbf{d}})L'(\hat{\mathbf{d}})^{T}$, where T signifies transposition of a column vector to a row vector. Second, construct the matrices $\mathbf{\Delta}_{pd}(\hat{\mathbf{d}})=\mathbf{g}_{\pi}(p,d,\hat{\mathbf{d}})+P(\hat{\mathbf{d}})D(\hat{\mathbf{d}})^{T}2/\sqrt{3}$ and $\mathbf{\Delta}_{dd}(\hat{\mathbf{d}})=\mathbf{g}_{\delta}(d,d,\hat{\mathbf{d}})-D(\hat{\mathbf{d}})D(\hat{\mathbf{d}})^{T}/3$ which are linear and quadradic, respectively, in the direction cosines. A conve-

nient basis for representing either the g_μ or $\tilde{g}_\alpha$ is then pp — **1**, $P(\hat{\mathbf{d}})P(\hat{\mathbf{d}})^T$; pd — $P(\hat{\mathbf{d}})D(\hat{\mathbf{d}})^T$, $\Delta_{pd}(\hat{\mathbf{d}})$; and dd — **1**, $D(\hat{\mathbf{d}})D(\hat{\mathbf{d}})^T$, $\Delta_{dd}(\hat{\mathbf{d}})$, where **1** signifies the appropriate identity matrix. Finally, the matrix dot products $\mathbf{g}_\mu(l,l',\hat{\mathbf{d}}_1)\cdot\mathbf{g}_{\mu'}(l,l',\hat{\mathbf{d}}_2)$ and $\tilde{\mathbf{g}}_\alpha(l,l',\hat{\mathbf{d}}_1)\cdot\tilde{\mathbf{g}}_{\alpha'}(l,l',\hat{\mathbf{d}}_2)$ for different directions $\hat{\mathbf{d}}_1$ and $\hat{\mathbf{d}}_2$ may be expressed in terms of the scalars $L(\hat{\mathbf{d}}_1)^T L(\hat{\mathbf{d}}_2)=\hat{\mathbf{d}}_1\cdot\hat{\mathbf{d}}_2$ and $[3(\hat{\mathbf{d}}_1\cdot\hat{\mathbf{d}}_2)^2-1]/2$ for the p and d cases, respectively; $L(\hat{\mathbf{d}}_1)^T\mathbf{\Delta}_{ll'}(\hat{\mathbf{d}}_2)L'(\hat{\mathbf{d}}_1)=2\,\hat{\mathbf{d}}_1\cdot\hat{\mathbf{d}}_2/\sqrt{3}$ and $-(\hat{\mathbf{d}}_1\cdot\hat{\mathbf{d}}_2)^2+2/3$ for the pd and dd cases, respectively; and $\mathbf{\Delta}_{ll'}(\hat{\mathbf{d}}_1)\cdot\mathbf{\Delta}_{ll'}(\hat{\mathbf{d}}_2)=10\,\hat{\mathbf{d}}_1\cdot\hat{\mathbf{d}}_2/3$ and $[21(\hat{\mathbf{d}}_1\cdot\hat{\mathbf{d}}_2)^2-2]/9$ for the pd and dd cases, respectively. In addition, there are scalar constants $L(\hat{\mathbf{d}})^T L(\hat{\mathbf{d}})=1$ and $\mathbf{1}\cdot\mathbf{\Delta}_{dd}(\hat{\mathbf{d}})=\frac{5}{3}$.

[1] J. C. Slater and G. F. Koster, Phys. Rev. **94**, 1498 (1954).

[2] L. F. Mattheiss, Phys. Rev. B **2**, 3918 (1970).

[3] D. J. Chadi and M. L. Cohen, Phys. Status Solidi B **68**, 405 (1975).

[4] L. F. Mattheiss and J. R. Patel, Phys. Rev. B **23**, 5384 (1981).

[5] P. B. Allen, J. Q. Broughton, and A. K. McMahan, Phys. Rev. B **34**, 859 (1986).

[6] D. A. Papaconstantopoulos, *Handbook of the Band Structure of Elemental Solids* (Plenum, New York, 1986).

[7] For tight-binding total-energy methods applied to surface relaxation and structure, see e.g., D. J. Chadi, Phys. Rev. B **29**, 7845 (1984); G. X. Xian and D. J. Chadi, *ibid.* **35**, 1288 (1987).

[8] W. A. Harrison, *Electronic Structure and the Properties of Solids* (Dover, New York, 1989), p. 479.

[9] L. Goodwin, A. J. Skinner, and D. G. Pettifor, Europhys. Lett. **9**, 701 (1989).

[10] A. T. Paxton, A. P. Sutton, and C. M. M. Nex, J. Phys. C **20**, L263 (1987).

[11] S. Sawada, Vacuum **41**, 612 (1990); M. Kohyama, J. Phys. Condens. Matter **3**, 2193 (1991).

[12] I. Kwon, R. Biswas, C. Z. Wang, K. M. Ho, and C. M. Soukoulis, Phys. Rev. B **49**, 7242 (1994).

[13] J. L. Mercer, Jr. and M. Y. Chou, Phys. Rev. B **47**, 9366 (1993).

[14] M. S. Tang, C. Z. Wang, C. T. Chan, and K. M. Ho, Phys. Rev. B **53**, 979 (1996).

[15] T. J. Lenosky, J. D. Kress, I. Kwon, A. F. Voter, B. Edwards, D. F. Richards, S. Yang, and J. B. Adams, Phys. Rev. B **55**, 1528 (1997).

[16] D. J. Chadi, in *Atomic Simulation of Materials Beyond Pair Potentials*, edited by V. Vitek and D. J. Srolovitz (Plenum, New York, 1988), p.309.

[17] J. L. Mercer, Jr. and M. Y. Chou, Phys. Rev. B **49**, 8506 (1994).

[18] R. E. Cohen, M. J. Mehl, and D. A. Papaconstantopoulos, Phys. Rev. B **50**, 14 694 (1994); M. J. Mehl, D. A. Papaconstantopoulos, R. E. Cohen, and M. M. Sigalas, in *Alloy Modeling and Design*, edited by G. Malcolm Stocks (Minerals, Metals, and Materials Society, Warrendale, PA, 1994), p. 25; M. J. Mehl, D. A. Papaconstantopoulos, and R. E. Cohen, Int. J. Thermophys. **16**, 503 (1995).

[19] L. Colombo, in *Annual Reviews of Computational Physics IV*, edited by D. Stauffer (World Scientific, Singapore, 1996), p. 147.

[20] O. K. Andersen and O. Jepsen, Phys. Rev. Lett. **53**, 2571 (1984); O. K. Andersen, O. Jepsen, and D. Glötzel, in *Highlights of Condensed Matter Theory*, edited by F. Bassani, F. Fumi, and M. P. Tosi (North-Holland, Amsterdam, 1985), pp. 59.

[21] M. H. F. Sluiter and P. P. Singh, Phys. Rev. B **49**, 10 918 (1994).

[22] D. Porezag, Th. Frauenheim, Th. Köhler, G. Seifert, and R. Kaschner, Phys. Rev. B **51**, 12 947 (1995).

[23] Th. Frauenheim, F. Weich, Th. Köhler, S. Uhlmann, D. Porezag, and G. Seifert, Phys. Rev. B **52**, 11 492 (1995); J. Widany, Th. Frauenheim, Th. Köhler, M. Sternberg, D. Porezag, G. Jungnickel, and G. Seifert, *ibid.* **53**, 4443 (1996).

[24] D. Sanchez-Portal, E. Artacho, and J. M. Soler, Solid State Commun. **95**, 685 (1995).

[25] J. Zhu, T. Diaz de la Rubia, L. H. Yang, C. Mailhiot, and G. H. Gilmer, Phys. Rev. B **54**, 4741 (1996).

[26] P. B. Rasband, A. P. Horsfield, and P. Clancy, Philos. Mag. B **73**, 71 (1996).

[27] P. B. Rasband, P. Clancy, and M. O. Thompson, J. Appl. Phys. **79**, 8998 (1996).

[28] See the last two paragraphs of the Appendix.

[29] M. Methfessel, Phys. Rev. B **38**, 1537 (1988).

[30] M. Methfessel, C. O. Rodriguez, and O. K. Andersen, Phys. Rev. B **40**, 2009 (1989).

[31] See, e.g., A. K. McMahan, Physica B & C **139&140B**, 31 (1986), Sec. 5.1.

[32] P. O. Löwdin, J. Chem. Phys. **19**, 1396 (1951).

[33] R. R. Sharma, Phys. Rev. B **19**, 2813 (1979).